Cell Calcium 45 (2009) 275–283

Contents lists available at ScienceDirect

Cell Calcium

journal homepage: www.elsevier.com/locate/ceca

Measuring mitochondrial and cytoplasmic Ca^{2+} in EGFP expressing cells with a low-affinity Calcium Ruby and its dextran conjugate

Camilla Luccardini[a,b,c,d,1], Aleksey V. Yakovlev[a,b,c,d,1], Mathias Pasche[e], Stéphane Gaillard[f], Dongdong Li[a,b,c], France Rousseau[d], Romain Ly[d], Ute Becherer[e], Jean-Maurice Mallet[f], Anne Feltz[d,**], Martin Oheim[a,b,c,*]

[a] *INSERM, U603, Paris F-75006, France*
[b] *CNRS, UMR 8154, Paris F-75006, France*
[c] *Université Paris Descartes, Laboratory of Neurophysiology and New Microscopies, 45 rue des Saints Pères, Paris F-75006, France*
[d] *ENS-CNRS, UMR 8544, Laboratoire de Neurobiologie, Département de Biologie, Ecole Normale Supérieure, 46 rue d'Ulm, Paris F-75005, France*
[e] *Physiologisches Institut, Universität des Saarlandes, Homburg D-66421 Germany*
[f] *ENS-CNRS, UMR 8642, Département de Chimie, Ecole Normale Supérieure, 24 rue Lhomond, Paris F-75005, France*

ARTICLE INFO

Article history:
Received 21 August 2008
Received in revised form
14 November 2008
Accepted 20 November 2008
Available online 24 January 2009

Keywords:
EGFP
Long-wavelength
Visible light
Red-emitting
Cytoplasmic calcium
Mitochondrial calcium
Synthesis
Co-localization
Dextran conjugate
In-situ characterization
Double-labeling
BAPTA
Buffer capacity
Low-affinity
Calcium microdomain

ABSTRACT

The limited choice and poor performance of red-emitting calcium (Ca^{2+}) indicators have hampered microfluorometric measurements of the intracellular free Ca^{2+} concentration in cells expressing yellow- or green-fluorescent protein constructs. A long-wavelength Ca^{2+} indicator would also permit a better discrimination against cellular autofluorescence than the commonly used fluorescein-based probes. Here, we report an improved synthesis and characterization of Calcium Ruby, a red-emitting probe consisting of an extended rhodamine chromophore (578/602 nm peak excitation/emission) conjugated to BAPTA and having an additional NH_2 linker arm. The low-affinity variant ($K_{D,Ca}$ ~30 μM) with a chloride in *meta* position that was specifically designed for the detection of large and rapid Ca^{2+} transients. While Calcium Ruby is a mitochondrial Ca^{2+}probe, its conjugation, via the NH_2 tail, to a 10,000 MW dextran abolishes the sub-cellular compartmentalization and generates a cytosolic Ca^{2+} probe with an affinity matched to microdomain Ca^{2+} signals. As an example, we show depolarization-evoked Ca^{2+} signals triggering the exocytosis of individual chromaffin granules. Calcium Ruby should be of use in a wide range of applications involving dual- or triple labeling schemes or targeted sub-cellular Ca^{2+} measurements.

1. Introduction

Imaging of the intracellular free calcium concentration ($[Ca^{2+}]_i$) in the presence of green- or yellow-emitting fluorescent proteins is limited by the spectral overlap between fluorescent Ca^{2+} indicators and fluorescent proteins as well as the reduced choice of red-emitting Ca^{2+} indicators. Surprisingly, this situation has evolved little since 2001 when Bolsover et al. [1] compared spectral separation in search of suitable Ca^{2+} indicators for combined Ca^{2+}/EGFP imaging. To meet the demand for an EGFP-compatible Ca^{2+} probe, we recently introduced Calcium Ruby Cl [2] (hereafter named Calcium Ruby for simplicity), a BAPTA substituted with Cl in *meta* position, conjugated to the Texas Red™/extended rhodamine (X-Rhod) moiety [3]. Similar to Rhod-2 and X-Rhod-1, but unlike for Calcium Crimson™, the BAPTA aromatic ring is an integral part of the rhodamine fluorophore of Calcium Ruby. As predicted for a substituted BAPTA, Calcium Ruby had an apparent dissociation constant for Ca^{2+} ($K_{D,Ca}$) of ~30 μM, measured at 20 °C and 0.1 M ionic strength [2]. When infused from a patch-pipette, we expect this indicator not to override the endogenous

* Corresponding author at: INSERM, U603, Paris F-75006, France. Tel.: +33 1 42 86 42 21; fax: +33 1 42 86 41 51.
** Corresponding author. Tel.: +33 1 44 32 38 88; fax: +33 1 44 32 38 87.
E-mail addresses: anne.feltz@ens.fr (A. Feltz), martin.oheim@univ-paris5.fr (M. Oheim).
[1] These authors contributed equally to this work.

0143-4160/$ – see front matter © 2008 Elsevier Ltd. All rights reserved.
doi:10.1016/j.ceca.2008.11.007

Ca^{2+} handling, because it introduces little Ca^{2+} buffer capacity [4], compared to typical endogenous Ca^{2+} binding ratios of >40, [5]. Assuming ~100 nM resting Ca^{2+} ($[Ca^{2+}]_0$) and 100–200 μM dye, $\kappa = K_{D,Ca}[B]_t/(K_{D,Ca} + [Ca]_0)^2 \approx 3$–6, where $[B]_t$ is the total buffer concentration (Ca^{2+}-bound and -free). Also, the low affinity for Ca^{2+} binding of Calcium Ruby should better match the amplitude of localized Ca^{2+} signals ('Ca^{2+} microdomains').

This paper describes an improved synthesis and characterization of the red-emitting Ca^{2+} Calcium Ruby, both as a free dye and as a 10,000 MW dextran conjugate. While the free dye preferentially labels mitochondria, the dextran conjugate remains cytosolic and is a faithful reporter of Ca^{2+} microdomains.

2. Materials and methods

2.1. Chemistry

Calcium Ruby N_3 was synthesized as previously described with some modifications [2], see Supplementary material online.

2.1.1. Preparation and purification of Calcium Ruby dextran

To prepare the amino compound, we worked in Staudinger conditions: a solution of Calcium Ruby N_3 (25 mg, 0.015 mmol) and triphenylphosphine (4 mg, 0.015 mmol) in tetrahydrofuran–water (1/1, 2 ml) was stirred for 2 h to give a solution of Calcium Ruby NH_2. Dextran (10,000 MW, 0–6 NH_2 per molecule, ref. D1860, Invitrogen, 25 mg, 0.0025 mmol) and *N*,*N*-carbonyldiimidazole (2.4 mg, 0.015 mmol) were dissolved in DMSO (3 ml) and stirred for 15 min [7–9]. The solution of Calcium Ruby NH_2 was added to dextran (6 eq./mol) solution. The mixture was stirred overnight, washed with cyclohexane (2 × 5 ml), concentrated and lyophilized. The residue was purified by gel filtration on a Sephadex G75 using water–*n*-propanol (40–1) as eluant. The collected fractions were pooled and lyophilized to give Calcium Ruby dextran (20 mg). Stock solution (1 mM) was prepared in a buffer containing (in mM) 10 HEPES and 150 NaCl (pH 7.5) and kept up to 6 months at 4 °C. For physiological use, we passed the product through two additional purification steps, first on a Sephadex G75 and then YM-10 (Amicon Danvers, MA), having 10 kDa-cutoff, to remove unbound dye.

2.2. Fluorescence microscopy and imaging spectroscopy

HEK-293, BON, and chromaffin cells, as well as glycinergic interneurons were prepared following standard protocols. Intracellular Ca^{2+} measurements were performed as detailed in the Supplementary experimental procedures. We used different fluorescence techniques.

2.2.1. Epifluorescence

EGFP/Calcium Ruby double-labeled cells were imaged on an inverted microscope (IX71, Olympus, Hamburg, Germany), equipped with a ×60 NA-1.45 oil-immersion objective (TIRFM PlanApochromat, Olympus), and a Poly V light source (TILL Photonics, Gräfelfing, Germany). After image-splitting with a dual-viewer device (W-viewer, hamamatsu, Hamamatsu City, Japan) and appropriate filtering (see Figure legends for details), images were captured on a QuantEM 512SC electron-multiplying CCD camera (16 μm × 16 μm pixel size, Photometrics, Tucson, AZ, USA), using MetaMorph (Molecular Devices).

2.2.2. Evanescent-wave imaging

For studying chromaffin-cell secretion, we used essentially the same system, with a solid-state (561 nm, 85 YCA, Melles Griot, Carlsbad, CA, USA) and Ar^+-ion laser (488 nm, 1885F12 Spectra-Physics, Mountain View, CA, USA) providing evanescent-field illumination through ×100 NA-1.45 planapochromatic objectives (Zeiss, Olympus) and TILL epi/TIRF dual-port condenser. Penetration depths were on the order of 150–200 nm. Images were detected, for depolarization experiments on a Micromax 512BFT camera (13-μm pixel size, Princeton Instruments Inc., Trenton, NJ, USA), or – for the flash-photolysis experiments – on an Andor iXon^{EM} (Pixel size 16 μm, Belfast, Northern Ireland). Acquisition rates were between 10 and 20 Hz, with exposure times between 80 and 37 ms.

2.2.3. Imaging spectroscopy

In-situ fluorescence excitation and emission spectra were recorded on a custom upright microscope with a TILL Polychrome II light-source. For imaging we mounted on one detection arm a Quantix-57 CCD camera (13 μm × 13 μm pixels, Photometrics) and, on the other arm, an imaging spectrograph (V8E, Zeutec, Rendsburg, Germany) and Cascade 128+ EMCCD detector (23 μm × 23 μm pixel size, 1.85-nm spectral sampling in the 484–680 nm range). Peak wavelengths are reported as the center wavelength ±95%-confidence interval from a fit of Gaussian distribution with the peak region of the spectrum measured on diffraction-limited organelle images or organelle-free cytoplasm.

2.2.4. Laser scanning microscopy

We assessed the sub-cellular localization of Calcium Ruby in BON cells doubly labeled with 60 μM Calcium Ruby and 10 nM Mitotracker green FM, (60 μM, pinocytically loaded, and 10 nM, 20 min incubation at 37 °C, respectively). For imaging, cells were fixed (4% paraformaldehyde, 10 min) and axial sections (dz = 0.3 μm) taken on a Yokogawa CSU10/Leica DM5000B spinning-disk confocal microscope, upon 491/635-nm dual-color excitation (Cobolt Calypso, 50 mW and Coherent Cube, 25 mW, respectively). Fluorescence was imaged through a ×40 HCX PL APO 1.25-0.75 oil objective (Leica) and detected with a CoolSNAP HQ2 CCD camera (6.45 μm pixel size, Photometrics).

Where indicated, electrophysiological recordings, membrane capacitance measurements or flash photolysis of caged Ca^{2+} accompanied image acquisition. See Figure legends and Supplementary experimental procedures for details.

2.3. Image analysis

We report, for all Ca^{2+}-indicator fluorescence, the average dF/F_0 value, measured from identified regions of interest (ROI), after the subtraction of extracellular background and averaged over the pixels of the ROI. For single chromaffin granules, the average fluorescence was taken in a 3 × 3-pixel ROI centered on the fluorescent spot. For the analysis of Ca^{2+} microdomains, we first averaged 100–200 pre-stimulus frames and divided the entire time-resolved Ca^{2+}-image stack by the average pre-stimulus image. In this way, we correct for local intensity differences resulting from the inhomogeneous membrane adhesion topography ('footprint'). We employed the coefficient of variation (CV) of the pixel-to-pixel fluorescence as a normalized measure of spatial heterogeneity. The CV is defined as the ratio of the standard deviation of the raw fluorescence intensity to the mean fluorescence (after subtraction of the average background signal) over all pixels of the footprint area. The footprint was outlined (average background plus 3-SD criterion) on the time-averaged pre-stimulus Calcium Ruby image and the region copied back in the time-lapse series to calculate the evolution with time of the spatial heterogeneity of the near-membrane Ca^{2+} signal, CV(t). Background was measured in a cell-free ROI identified on a bright-field image. An increase in the CV as defined here indicates that the spatial signal fluctuations grow faster than the average signal, indicative of an increase in 'graininess' of the fluorescence.

2.3.1. Co-localization

We first quantified the absence of spectral cross-talk and co-localization using the spectral separability index X_{ijk} and a modified Pearson's correlation coefficient, r_{12} [6]. Mitotracker green FM and Mitotracker Deep Red (100 nM each) co-loading in the absence of Calcium Ruby and a scrambled image plane rotated by 90° served as positive and negative controls, respectively. See Supplementary Table T1 for details.

2.3.2. Statistics

Ensemble averages data give mean ± SD, unless otherwise stated. For all experiments, samples were from at least three independent preparations; n is the number of cells, unless otherwise indicated. Statistical significance was established with tests suited for normally and non-normally distributed data, and paired tests used where appropriate. P values <0.05 were considered significant.

3. Results and discussion

3.1. Calcium Ruby is a Ca^{2+}-selective indicator compatible with EGFP labeling

Calcium Ruby N_3 [2] was reduced to Calcium Ruby NH_2, which was coupled with an activated aminodextran (10 kDa, presenting 5–6 amines/mol) to give a ~13 kDa molecular-weight Calcium Ruby dextran conjugate, having ~7 nm size [10]. The syntheses of Calcium Ruby and its dextran conjugate are outlined in Supplementary Fig. S1.

Calcium Ruby NH_2 with a chloride in *meta* position displayed an absorption maximum 579 nm and a fluorescence peak at 598–602 nm, with a shoulder near 650 nm. Its absorption and emission spectra are both red-shifted compared to that of EGFP with peaks at 488 nm and 507–509 nm, respectively [11], Fig. 1A. Using the spectral separability index X_{ijk} [6], we estimated that for an equimolar mixture of Calcium Ruby and EGFP, below 1% of the fluorescence detected in the EGFP and Calcium Ruby channel are due to cross-talk, see Supplementary Table T1. Indeed, no cross-excitation or fluorescence bleed-through were detectable when mouse embryonic spinal cord motoneurons expressing EGFP controlled by regulatory elements of the glycine transporter 2 (GlyT2) gene were whole-cell patch-clamped and loaded with 30 μM Calcium Ruby in the pipette and imaged in dual-color epifluorescence, Fig. 1B.

In vitro, Calcium Ruby NH_2 was virtually non-fluorescent in the absence of divalent cations. Ca^{2+} binding increased its peak fluorescence about 50-fold ($dF/F_0 = 51.4 \pm 7.9$, $n = 4$), Fig. 1C, left panel, with only negligible variation in peak emission (~1 nm red-shift per log unit [Ca^{2+}], see Supplementary Fig. S2, panel A). We found an apparent dissociation constant of 29.6 ± 3.55 μM (mean and 95% confidence interval, $n = 4$, at 25 °C and 0.1 M ionic strength, similar to the originally reported value. The Hill coefficient was 0.98 ± 0.21 ($n = 4$) suggesting that one Ca^{2+} ion is bound per molecule, as expected for BAPTA. The fluorescence of known concentrations Sulforhodamine 101 and Rhodamine B was compared with Ca^{2+}-bound and Ca^{2+}-free Calcium Ruby to provide an estimate of $\varphi_{CaB} = 0.42 \pm 0.03$ ($n = 4$) for the *in vitro* quantum yield at saturating [Ca^{2+}] (329 μM). In contrast, in Ca^{2+}-free solution, the quantum yield of Calcium Ruby fluorescence was $\varphi_B = 0.026$, corresponding to a 16-fold increase of the total fluorescence upon Ca^{2+} binding.

Cuvette titration of Calcium Ruby 10,000-dextran conjugate revealed identical properties for the dextran conjugate: with a $K_{D,Ca} = 31.7 \pm 6.44$ μM, a fractional fluorescence increase upon Ca^{2+} binding $dF/F_0 = 52 \pm 17.6$, and a Hill coefficient 0.96 ± 0.20 (*in vitro*, $n = 3$) the dextran was indistinguishable from the unconjugated fluorophore (data not shown).

Once loaded intracellularly, Ca^{2+} indicators are exposed to an intracellular saline of high ionic strength and often fluctuating composition. Under most circumstances, Mg^{2+} is the most abundant divalent metal ion. Adding 2 or even 5 mM Mg^{2+} in our Ca^{2+} titrations neither affected the apparent $K_{D,Ca}$ nor the dynamic range of Calcium Ruby. We also assessed the sensitivity of Calcium Ruby to transition metal cations according to Nolan et al. [12]. Briefly, we first measured the fractional fluorescence change (dF/F_0) upon adding 50 μM of Zn^{2+}, Mn^{2+}, Ni^{2+} or Co^{2+} to a solution containing nominally zero Ca^{2+}, 100 mM KCl and 30 mM MOPS (pH 7.2, 25 °C), Fig. 1C, middle panel, grey bars. Calcium Ruby was highly selective for Ca^{2+}, with significant fluorescence only in the presence of Mn^{2+} or Zn^{2+}. We then added to the same solution another 50 μM Ca^{2+} to test if the dye was still complexing Ca^{2+}, white bars. Binding to transition metal ions rendered Calcium Ruby Ca^{2+}-insensitive. Co^{2+} quenched Calcium Ruby fluorescence to <6.5% of its control value and was the most efficient among these quenchers. It can thus be used for the estimation of the non-Ca^{2+} related red cellular fluorescence in calibrated biological Ca^{2+} measurements.

Finally, in the presence of 24 μM Ca^{2+} Calcium Ruby fluorescence varied only moderately around physiological pH, with an apparent pK_a of 6.22 ± 0.07 ($n = 4$), Fig. 1C, right. This value is close to the values reported for BAPTA (5.97 and 6.36, [13,14]), although we could not resolve two steps. In line with this observation, the titration of the structurally similar Texas Red™ fluorophore against protons in the pH range of 6.0–8.0 did not reveal appreciable fluorescence changes, Supplementary Fig. S2, panel B, suggesting that protons affect Ca^{2+} chelating rather than the Calcium Ruby fluorophore directly. Thus, the BAPTA aromatic amines are largely unionized at physiological pH, making Calcium Ruby fluorescence relatively insensitive to small variations around pH 7.4. The indicator may be partially protonated when the dye is localized in acidic cellular compartments.

Taken together, the photophysical properties of both Calcium Ruby and its dextran conjugate are typical for an extended rhodamine chromophore. As intended for an indicator designed to measure rapid and highly localized Ca^{2+} microdomains, its affinity for Ca^{2+} is of the order of 30 μM, in the range predicted for a chloride-substituted BAPTA moiety [2].

The high Ca^{2+} selectivity and low pH dependence make Calcium Ruby a promising candidate for Ca^{2+} measurements under various conditions prevailing in an intracellular environment. With a molar extinction of $\varepsilon_{580} \sim 100{,}000\ M^{-1}cm^{-1}$ [2] the brightness of Calcium Ruby can be estimated as $B_{CaRuby} = \varepsilon \times \varphi_{CaB} = 42{,}000\ M^{-1}\ cm^{-1}$, compared to ~34,000 $M^{-1}cm^{-1}$ for both Calcium Crimson™ and Calcium Orange™ (no data available for X-Rhod-1 and Rhod-2). The brightness of Ca^{2+}-bound Calcium Ruby is comparable to that of EGFP ($B_{EGFP} = 42{,}840\ M^{-1}cm^{-1}$), which – along with the negligible spectral cross-talk – facilitates dual-color detection. The large molar extinction and high quantum yield in the presence of Ca^{2+} rank Calcium Ruby among the brightest long-wavelength Ca^{2+} indicators available.

3.2. Calcium Ruby is sequestered into mitochondria

Calcium Ruby (MW = 1004 g/mol, with a size of ~1.5 nm) was virtually membrane-impermeable to HEK293 or BON cells, even when present in the cell culture medium over 24 h. However, we noted a faint but resistant plasma membrane staining (data not shown).

We loaded Calcium Ruby into cells using different techniques (pinocytic uptake followed by osmotic shock, single-cell electroporation, or – preferentially – whole-cell patch-clamp, see Supplementary materials). Whatever the technique used, Calcium Ruby showed a propensity to accumulate in small granular organelles, see, e.g., Supplementary Movie 1 for a time-lapse image

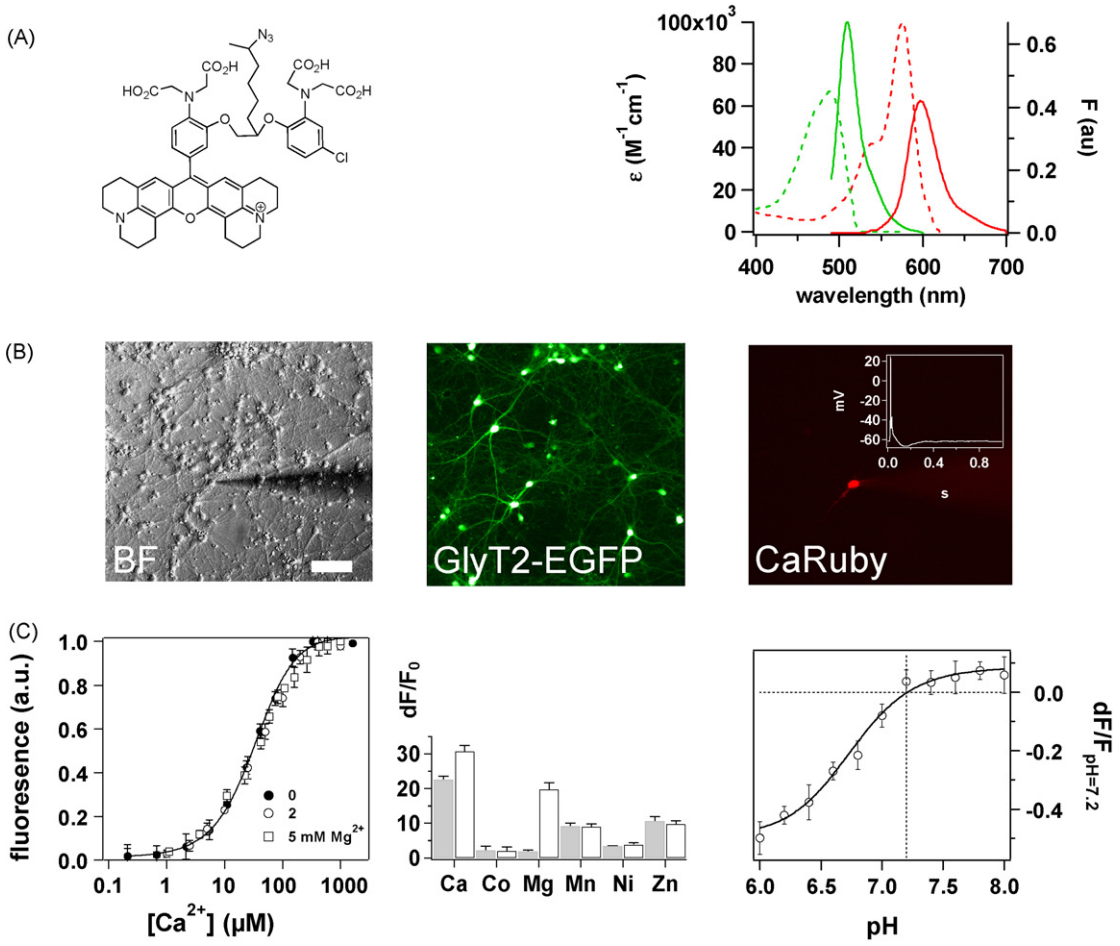

Fig. 1. Calcium Ruby permits dual-color imaging with no detectable cross-talk from EGFP labeling. (A) Left, chemical structure of Calcium Ruby-N_3. Right, absorption (dashed) and fluorescence emission (solid) spectra of EGFP (green) and Calcium Ruby (red) in a solution containing 329 μM free [Ca^{2+}], slit-width: 5 nm, 1-nm scan. (B) Bright-field (BF) and EGFP fluorescence (*GlyT2-EGFP*) image of mouse spinal cord neurons at DIV 21 expressing EGFP under the GlyT2 promoter. An EGFP-labeled interneuron was patch-clamped and filled with 30 μM Calcium Ruby monochloride salt. The patch-pipette is seen as a weakly fluorescent cone on the right. Inset: stable action potentials could be recorded for more than 1 h in the presence of 30 μM of Calcium Ruby. Average of the action potential overshoot: 25.9 ± 0.3 mV (n = 10). Fluorescence images were captured at 1 Hz on a CoolSNAP-ES CCD camera (RoperScientific, 6.45 μm pixel size) using a LCPLFL × 20 RC NA-0.4 long-working distance objective (Olympus). Filters were, for EGFP: (ex., dic., em.) HQ470/40, Q495LP, HQ525/50m and for Calcium Ruby, D545/30, Q570LP, HQ620/60m. Scale bar is 50 μm. (C) Calcium Ruby divalent-cation selectivity and pH sensitivity. Left, plot of the normalized Calcium Ruby peak fluorescence in the 550–700-nm range, upon excitation at 535 nm, against [Ca^{2+}] in a buffer containing (in mM): 30 MOPS, 100 KCl, 10 NTA as well as zero (solid dots), 2 (circles) or 5 mM $MgCl_2$ (rectangles), 25 °C, pH 7.2. Data are corrected for blank run, subtracted with fluorescence at zero Ca^{2+} and normalized to peak at 602 nm. Error bars give *SD*, solid line is a fit of Hill's equation with the data for zero Mg^{2+} (slope 0.98 ± 0.21 and $K_{D,Ca}$ = 29.6 ± 3.55. Middle, grey bars, relative fluorescence changes (dF/F_0) in the presence of 50 μM of Ca^{2+}, Co^{2+}, Mg^{2+}, Mn^{2+}, Ni^{2+} and Zn^{2+}. White bars represent dF/F_0 after adding 50 μM Ca^{2+} to the solution already containing 50 μM of the divalent cation indicated. Emission was monitored in the 550–700-nm range upon 535-nm excitation. Titration buffer contained (in mM) 0.01 Calcium Ruby, 100 KCl and 30 MOPS. Right, evolution with pH of Calcium Ruby peak fluorescence (n = 4, ex./em. = 535/602 nm, 25 °C). Buffer contained (in mM) 0.01 Calcium Ruby Cl, 100 KCl, 10 NTA ([Ca^{2+}] = 25 μM) and 30 mM MES (pH 6.0–6.8) or MOPS (pH 7.0–8.0). Fitting Hill's equation with the average data yields a pK_a = 6.22 ± 0.07. Data are normalized to fluorescence at pH 7.2. (For interpretation of the references to color in this figure legend, the reader is referred to the web version of the article.)

series of a spinal cord interneuron that was whole-cell patch-clamp loaded.

This sequestration into organelles might also explain the reduced dynamic range observed upon Ca^{2+} binding of Calcium Ruby *in situ*: when bulk-loading the indicator into BON cells using pinocytic uptake followed by osmotic shock, and permeabilizing the plasma membrane with the Ca^{2+} ionophore A23187 and integrating over the entire spectrum, we found a dF/F_0 = 0.56 ± 0.20, (min = 0.43, max = 0.83, n = 8), for zero and 2 mM extracellular Ca^{2+}, almost 30 times less than *in vitro* (16-fold change, see above). Yet, Calcium Ruby still performed ~2-fold better than Xrhod-1 under identical conditions (0.26 ± 0.19, min = 0.02, max = 0.64, n = 7, P < 0.001, data not shown).

What is the identity of the sub-cellular compartment labeled by Calcium Ruby? Like other rhodamine-based indicators, Calcium Ruby carries a delocalized positive charge, and we speculated that this charge could drive its accumulation in the negatively charged mitochondrial matrix. To ascertain the mitochondrial identity of the sub-cellular compartment labeled by Calcium Ruby we counterstained BON cells with different organelle markers that could be imaged with negligible spectral cross-talk X_{ijk}, Supplementary Table T1. Confocal images of Calcium Ruby and Mitotracker Green FM fluorescence were highly correlated when measuring a modified Pearson's coefficient (r_{12} = 0.97 ± 0.03, 40 cells, see Supplementary Movie M2), not significantly different from the positive control value obtained in BON cells double-stained with two mitochondrial markers (MitoTracker Green FM/Mitotracker Deep Red 633, r_{12} = 0.98 ± 0.01, n = 48, n.s.) and much higher than the lower meaningful limit of correlation calculated from randomly selected and scrambled red and green image planes (r_{12} = 0.15 ± 0.05, n = 6, P < 0.01), Fig. 2A. Controls with Calcium Ruby and Mitotracker Deep Red 633 or ER Tracker blue/white DPX corroborated the mitochondrial localization of Calcium Ruby (data not shown).

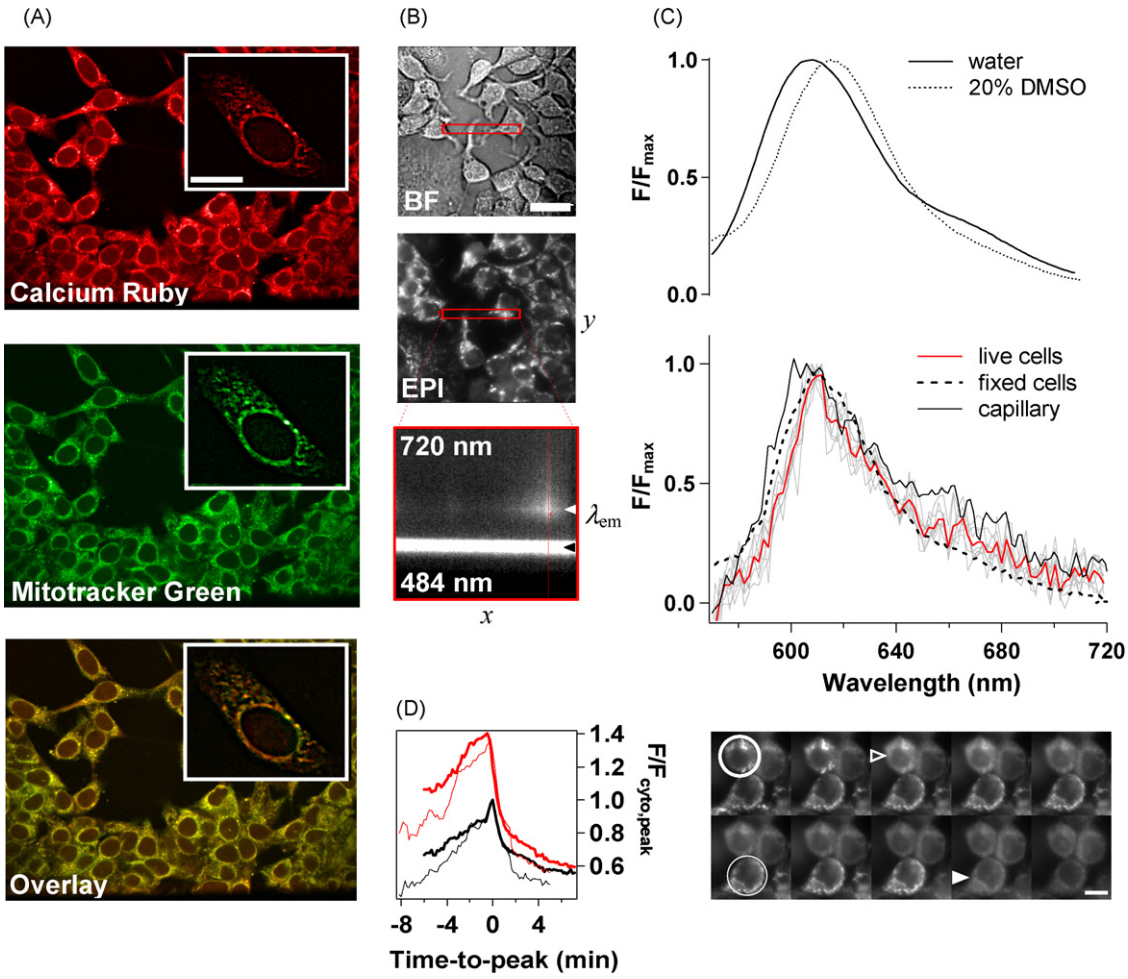

Fig. 2. Calcium Ruby fluorescence reports mitochondrial Ca^{2+}. (A) Representative planes of a confocal image z-stack of Calcium Ruby (top) and Mitotracker Green FM (middle) double-labeled BON cells. Bottom panel shows pseudo-color overlay. Pearson's correlation coefficient was 0.97 ± 0.03, indicating the almost complete overlap of both fluorescence labels. Inset, single cell at larger magnification, after nearest-neighbor deconvolution. Note the tubular organelles in the perinuclear region. For confocal imaging, a Di01T405/488/568/657 quadruple dichroic reflected the 491 and 561-nm laser lines. Fluorescence of Calcium Ruby and Mitotracker Green were detected through a Semrock 617/63 and HQ520/35m emission band-pass (Chroma). Scale is 10 μm. (B) Top, bright-field (BF) image of BON cells bulk-loaded with Calcium Ruby following osmolysis of pinocytic vesicles. Red box identifies region apertured by the entry slit of the imaging spectrograph. Scale is 20 μm. Middle, 560/620 nm epifluorescence image of the same field, dichroic 585DCXR. Bottom, background-corrected spectral image (x vs. λ_{em} in the range 484–720 nm) of the boxed region upon epifluorescence excitation (black arrow). Spectral resolution is 1.85 nm. White arrowhead identifies fluorescence emission spectrum of granular fluorescence as shown in the middle panel, black arrowhead points to the residual transmitted excitation light ($\lambda_{ex} = 560 \pm 9$ nm). Spectrum in (C) is measured along the red line after background subtraction. Top, *in vitro* emission spectrum of Calcium Ruby in aqueous solution (solid) and 20% DMSO (dotted). Bottom, *in situ* emission spectra. Grey and red curves are individual organelles and ensemble average ($n = 8$). Black, Calcium Ruby spectrum measured from fixed cells (dotted) and 20 μM Calcium Ruby in a 20 μm × 50 μm glass capillary (solid) for comparison. (D) Induction of mitochondrial transition pore opening by Ca^{2+} overload. Left, Evolution with time of Calcium Ruby fluorescence in two neighboring BON cells (thick and thin lines, respectively) pinocytically loaded with 30 μM Calcium Ruby and challenged by the application of the Ca^{2+} ionophore A23187 (50 μM), in the presence of 4 mM $CaCl_2$. Graph displays mitochondrial (red) and cytoplasmic (black) regions of interest. Traces are normalized to peak cytoplasmic fluorescence ($F_{cyto,peak}$) and aligned to the time of peak to better visualize their comparable time-course. Right, image planes extracted from a time-series showing mitochondrial transition pore opening occurring consecutively in two neighboring cells, as indicated by arrowheads. Cells circled by thick and thin lines correspond to thick and thin traces on the left panel, respectively. Time between frames is 1 min. Scale 10 μm. (For interpretation of the references to color in this figure legend, the reader is referred to the web version of the article.)

Functional arguments further supported the notion that Calcium Ruby is a mitochondrial Ca^{2+} probe, Fig. 2B. Organelle-sequestered Calcium Ruby had a red-shifted peak emission (612.0 ± 0.5 nm, $n = 8$ cells) compared to a solution of 20 μM Calcium Ruby in 2 mM $CaCl_2$ or 1 mM Calcium Ruby in methanol, respectively, measured in a 20 μm × 100 μm quartz capillary (606.7 ± 0.7 nm and 605.9 ± 1.19 nm, respectively, $n = 2$ and 4, $P < 0.01$ both). We observed a comparable red-shift (612.0 ± 0.2 nm, $n = 7$) when removing the non-sequestered cytoplasmic dye from the cytoplasm through 0.05% Triton-X100 permeabilization, wash and fixation, indicating that the spectrally shifted dye fraction was retained and not washed from the cytoplasm, Fig. 2C. These wavelength shifts are compatible with values observed by others for rhodamine 123, tetramethylrhodamine methyl ester (TMRM), and tetramethylrhodamine ethyl ester (TMRE) in isolated mitochondria [15–17]. Interestingly, the addition of 20% DMSO instead of water to a Calcium Ruby stock solution had as an effect a similar red-shift, raising the possibility that solvatochromism contributes, at least in part, to the shifted emission of mitochondrially sequestered Calcium Ruby.

Mitochondrial and cytoplasmic Ca^{2+} imaging further substantiated the role of Calcium Ruby as a reporter of mitochondrial Ca^{2+}. Mitochondria sequester large cytoplasmic Ca^{2+} loads but Ca^{2+} accumulation causes reactive oxygen species production, leads to oxidative stress and, in the case of overload, to a breakdown of Ca^{2+} homeostasis through a mechanism known as mitochondrial

permeability pore transition, MPT [18]. To determine if excess mitochondrial Ca^{2+} affected Calcium Ruby fluorescence, we imaged BON cells following Ca^{2+} ionophore administration [19–21] in a solution containing 4 mM $CaCl_2$. A23187 (50 μM) promoted the equilibration between cytoplasmic and mitochondrial compartments: mitochondrial ($[Ca^{2+}]_m$) and cytoplasmic Ca^{2+} ($[Ca^{2+}]_i$) initially increased together, before an abrupt drop in $[Ca^{2+}]_m$ coincided with a peak in $[Ca^{2+}]_i$, indicating pore opening, dissipation of $\Delta\Psi_m$ and the release of the mitochondrially accumulated Ca^{2+}, Fig. 2D. Eventually, Calcium Ruby fluorescence dropped in both compartments, compatible with the slow export of Ca^{2+} across the plasma membrane ($\tau = 36.7 \pm 0.04$ s, $n = 35$ cells). Although mitochondrial alkalization upon MPT could potentially change fluorescence (see Fig. 1C), the mitochondrial Calcium Ruby signal rather dropped than increased, indicating that pH effects, if present, were negligible compared to the loss of fluorescence due to the drop of $[Ca^{2+}]_m$ or intracellular dye relocation in response to MPT.

In summary, our experiments indicate that Calcium Ruby coexists in cytoplasmic and mitochondrial compartments and that most of its fluorescence under physiological conditions derives from mitochondrial Ca^{2+}. The detection of $[Ca^{2+}]_m$ is facilitated by the indicator's low Ca^{2+}-binding affinity and its tendency to concentrate in mitochondria. Our data further reveal the absence of Calcium Ruby fluorescence from the nucleus. The data obtained in fixed and permeabilized cells indicate the existence of a membrane-bound and fluorescent fraction of the indicator that is retained even after fixation.

3.3. *Imaging micromolar cytoplasmic Ca^{2+} signals with Calcium Ruby dextran in bovine adrenal chromaffin cells*

Mitochondria can accumulate amphiphilic cations up to a size of ~1.5 kDa [22,23]. Larger molecules should not be taken up and hence report cytoplasmic $[Ca^{2+}]$. We designed Calcium Ruby to be linked via an amidic bond to target molecules and we here used this NH_2 linker to couple several fluorophores to a large molecular-weight dextran. The expected size of this dextran conjugate is of the order of 13,000 Da and hence should prevent mitochondrial sequestration, see Supplementary material. We validated this strategy by imaging micromolar cytoplasmic Ca^{2+} signals that trigger neuroendocrine secretion.

Chromaffin cells are specialized neurosecretory cells that secrete epinephrine, norepinephrine and endorphins in response to voltage-gated Ca^{2+} entry. Maintained or repeated depolarization triggers a phasic secretory response synchronized with Ca^{2+} channel opening, followed by a slower sustained component [24]. Phasic release is triggered by localized Ca^{2+} gradients, which form around the mouth of open ion channels and reach a peak $[Ca^{2+}]_i$ in the 10–100 μM range [25]. Due to the ~300-nm size of chromaffin granules [26], single secretory events can be visualized using evanescent-field microscopy [27,28].

For imaging the Ca^{2+}-regulation of single-vesicle exocytosis we labeled chromaffin granules by transiently expressing a turquoise-green ('teal') fluorescent neuropeptide-Y (NPY) mTFP construct and patched cells with 200 μM Calcium Ruby dextran in the pipette. We monitored the intracellular near-membrane Ca^{2+} signal and single-vesicle dynamics with interleaved 488/568-nm dual-color evanescent-field excitation [29]. Phasic and sustained releases were evoked with a series of depolarizing steps [24] and flash photolysis of caged-Ca^{2+}, respectively. Simultaneous whole-cell patch-clamp recordings of the membrane capacitance changes (ΔC_m) measured the bulk secretory response [30]. Single exocytic events were recognized, after tracking single green fluorescent spots and measurement of their intensity over time, as a rapid intensity drop, Fig. 3A.

The photostability of both mTFP and Calcium Ruby allowed us to acquire time-lapse movies with more than 1000 frames, see Supplementary Movie M3. A series of four 100-ms step depolarizations evoked robust changes in the average sub-plasmalemmal Calcium Ruby fluorescence measured in the cellular footprint ($dF/F_0 = 0.54 \pm 0.14$, 0.57 ± 0.08, 0.72 ± 0.13 and 0.52 ± 0.07, for the first, second, third and fourth depolarization, respectively, Fig. 3B). In contrast, the four 10-ms pulses barely affected the average $[Ca^{2+}]_i$ level ($dF/F_0 = 0.03 \pm 0.05$, min = 0.00, max = 0.19, $n = 7$). Pre-stimulus baseline fluctuations of the average near-membrane Ca^{2+} signal were not significantly different from these dF/F_0 values, 0.02 ± 0.04 ($n = 7$, n.s.). Pulse trains triggered global sub-plasmalemmal Ca^{2+} transients that summed up to a total peak $dF/F_0 = 1.40 \pm 0.36$, mean ± SEM, min = 0.89, max = 3.37, and decayed exponentially ($\tau = 1.61 \pm 0.29$ s) leaving a residual Ca^{2+} of $dF/F_0 = 0.56 \pm 0.25$, $n = 7$ cells. Removing Ca^{2+} from the extracellular saline abolished both depolarization-evoked currents and Ca^{2+} transients ($dF/F_0 = 0.04 \pm 0.02$, $n = 6$ cells, $P < 0.001$) as well as Ca^{2+}-triggered membrane capacitance (ΔC_m) increases, suggesting that Calcium Ruby detected voltage-gated Ca^{2+} influx rather than Ca^{2+} release from intracellular stores and that this Ca^{2+} influx across the plasma membrane provided the trigger for exocytosis, Fig. 3B, grey traces.

At the sub-cellular level, both 10- and 100-ms step depolarizations evoked a spatially inhomogeneous pattern of near-membrane fluorescence. The plot over time of the coefficient of variation of the measured fluorescence intensity across pixels of the footprint region of the cell illustrates that the depolarization-evoked heterogeneity of the Calcium Ruby fluorescence coincided with voltage-gated Ca^{2+} channel opening. Spatial heterogeneity decayed within tens of ms, much faster than the average near-membrane dF/F_0 Ca^{2+} signal, suggestive of the rapid dissipation of standing Ca^{2+} gradients after ion channel closure. Extracellular background did not display comparable CV variations, excluding a contribution from laser or detector noise (data not shown). Omitting Ca^{2+} from the extracellular fluid abolished both the evoked Ca^{2+} increase and deflection in the CV trace, suggesting that the low affinity of Calcium Ruby is suited to detect spatial heterogeneity of the depolarization-evoked Ca^{2+} signal, Fig. 3C, right. Corroborating this interpretation, flash photolysis of the photolabile chelator nitrophenyl-EGTA (NP-EGTA, that selectively binds Ca^{2+} with ~80 nM affinity and releases it rapidly upon photolysis) producing a similar-amplitude average Ca^{2+} signal ($dF/F_0 = 0.87 \pm 0.17$, $n = 6$, for the UV-flash vs. 0.99 for the depolarization-evoked peak dF/F_0) resulted in a ~10% reduction in spatial heterogeneity, compared to the pre-stimulus fluorescence ($\Delta CV/CV = -0.12 \pm 0.07$, $n = 6$). Thus, unlike in the depolarization experiments, Calcium Ruby reported a uniform increase in near-membrane Ca^{2+} following flash photolysis of caged Ca^{2+}, Fig. 3C, middle. Omitting NP-EGTA from the patch-pipette and repeating the flash experiment in cells loaded with Calcium Ruby alone failed to produce detectable fluorescence or *CV* changes, excluding a flash artifact (data not shown). Finally, when acquiring interlaced 488-/561-nm evanescent-wave dual-color fluorescence, we observed that CV changes in small image sub-regions reached much higher amplitude that the average near-membrane Ca^{2+}. Interestingly, near-membrane chromaffin granules are seen as dark spots on the Calcium Ruby images, and fluorescently labeled granules filled these gaps on the corresponding mTFP image (see Supplementary Fig. S3 for details), indicating that our Calcium-Ruby dextran was stable in the intracellular chemical microenvironment and was excluded from the vesicle lumen, Fig. 3D.

Together, although still limited by their diffraction-limited spatial and temporal resolution, our experiments demonstrate that the dextran conjugate of Calcium Ruby is well suited for recording localized micromolar near-membrane Ca^{2+} gradients associated with phasic release.

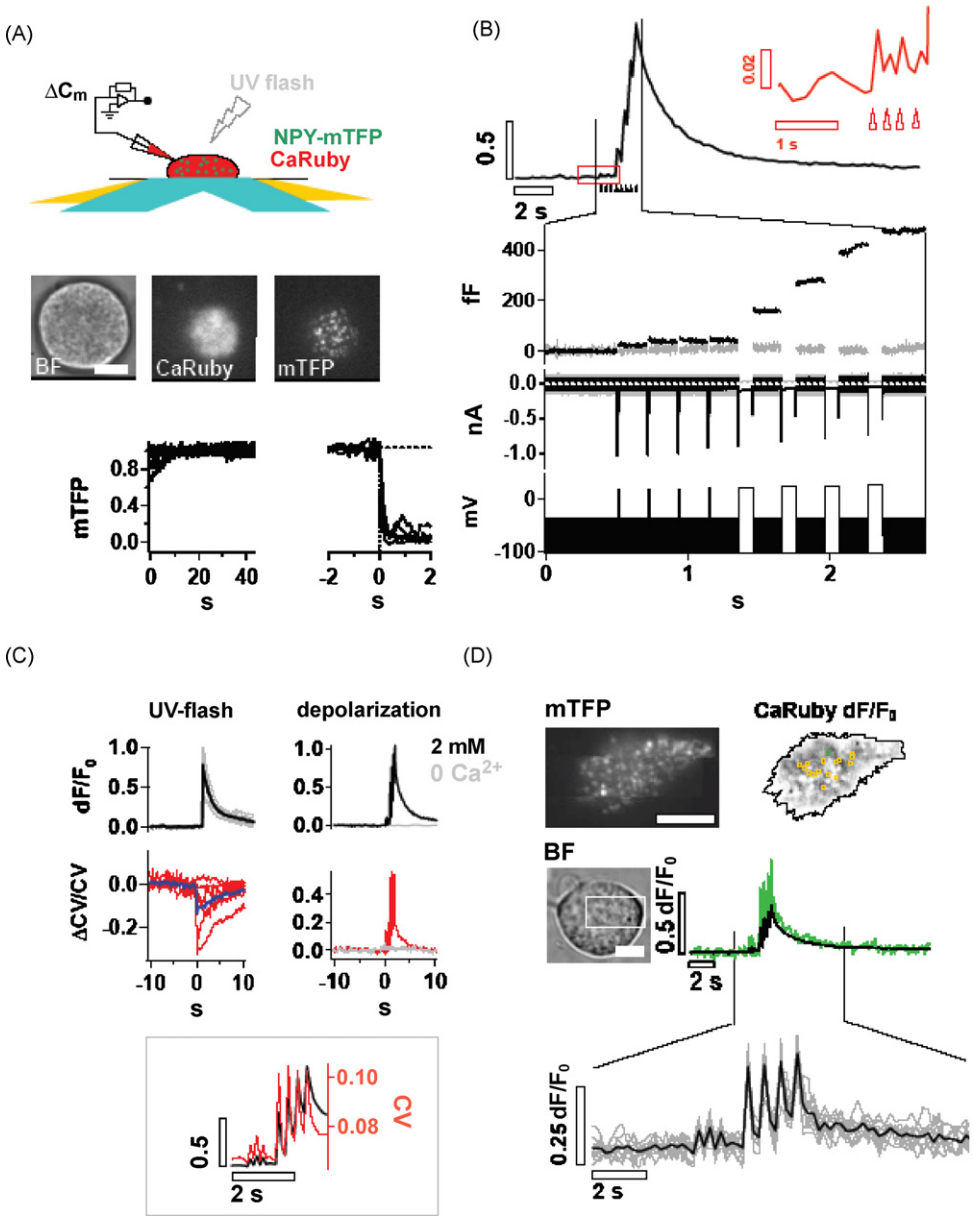

Fig. 3. Imaging Ca^{2+} microdomains with Calcium Ruby 10,000-MW dextran. (A) Left, top, schematic representation of alternate 488/561-nm dual-color TIRF imaging and whole-cell patch recording of chromaffin-granule exocytosis and near-membrane Ca^{2+}-dynamics. Cells expressing a green fluorescing NPY-mTFP construct were loaded with 200 μM Calcium Ruby dextran by infusion from the patch-pipette and secretion was stimulated with step depolarizations or flash photolysis of caged Ca^{2+} (UV-flash). Membrane capacitance (ΔC_m) provided a read-out for bulk exocytosis. Middle, example of a bovine adrenal chromaffin cell in bright-field (BF), and – 2 min after going whole-cell – upon 488-nm (mTFP) and 561-nm (CaRuby) evanescent-wave excitation. Exposure times were 80 ms. Scale is 5 μm. Bottom, time-resolved fluorescence traces from single NPY-mTFP labeled chromaffin granules, identifying granules unaffected by stimulation ($n = 11$, left), and exocytic events ($n = 5$, right). Traces are corrected for photobleaching and normalized to pre-stimulus fluorescence, and, for released granules, aligned to the time-point of fusion. (B) Top, example of the evolution with time of the average near-membrane Calcium Ruby fluorescence in the cellular 'footprint' region, in response to 4×10 ms and 4×100 ms depolarizations, same cell as in panel A. Red trace shows enlarged view of the boxed time-window. Arrowheads indicate time-points of 10- and 100-ms depolarizations. Vertical scale gives dF/F_0 fluorescence change. Bottom, membrane potential and current, along with the bulk secretory response, in the presence (black) and absence (grey) of extracellular Ca^{2+}. Current and voltage baselines appear large because of the sinusoidal modulation around holding potential, used to measure ΔC_m. (C) Analysis of the 'graininess' of the evoked Ca^{2+} signal in terms of the coefficient of variation shows the expected homogenous Ca^{2+} increase following flash photolysis of caged Ca^{2+} (UV-flash), but a markedly increased heterogeneity for a depolarization-evoked Ca^{2+} influx, despite comparable amplitude of the transients. Grey traces on right panels confirm absence of responses in zero Ca^{2+}. Red and blue CV traces show individual cells and population average. Boxed, superposition of $CV(t)$ and dF/F_0 responses. (D) Top, 488-nm (mTFP), and 561-nm (CaRuby) excited evanescent-field excited fluorescence following depolarization. Due to exclusion of the dextran conjugate, chromaffin granules appear as white spots on the dF/F_0 image as opposed to regions of high Ca^{2+} that are seen as dark pixels. Middle, evolution with time of dF/F_0 fluorescence, in response to a train of depolarizing pulses as above, for the entire footprint (black) and the diffraction-limited region identified on the Calcium Ruby image above (green). Bottom, dF/F_0 local Ca^{2+} signals (grey traces) read-out from diffraction-limited ROIs as identified in orange on the top image and their population average (black). Local Ca^{2+} domains add another ~25% increase to the global Ca^{2+} signal, are restricted to very confined regions and decay rapidly, within one frame (37 ms). Scale bars: 5 μm. See Supplementary material for experimental details. (For interpretation of the references to color in this figure legend, the reader is referred to the web version of the article.)

4. Conclusion

We synthesized and characterized the amino- and dextran-coupled form of a long-wavelength emitting low-affinity Ca^{2+} indicator based on a Texas Red™ linked to a chloride-substituted BAPTA Ca^{2+} chelator. The development of Calcium Ruby was motivated by the desire to perform dual-color live-cell Ca^{2+} imaging in fluorescent protein (FP) expressing cells, which has been hindered by the overlapping absorption and emission spectra of the yellow-green emitting FPs used in many plasmids and popular fluorescein-based Ca^{2+}-indicator dyes [1]. Additional motivations were that live cells are less sensitive to longer-wavelength excitation and that autofluorescence excitation is typically reduced under these conditions. Red-emitting Ca^{2+} dyes also should be beneficial for *in vivo* imaging, because longer-wavelength light is less susceptible to scattering and penetrates tissue more easily.

An ideal red-emitting $[Ca^{2+}]_i$ indicator for measuring microdomain Ca^{2+} concentration ($[Ca^{2+}]_\mu$) would have the following properties.

Ca^{2+} should bind with a dissociation constant ($K_{D,Ca}$) of 1–100 μM and fast association constant k_{on} at pH 7.4. Such a $K_{D,Ca}$ would approximately match the expected range for $[Ca^{2+}]_\mu$ (see, e.g., special issue vol. 40 (4–5), 2006, of *Cell Calcium* for a comprehensive review) and maximize the sensitivity to detect sites of local signaling domains.

The indicator should be pH-insensitive in the physiological range and discriminate between Ca^{2+} and other divalent cations, particularly Mg^{2+}.

It should fluoresce strongly, with a brightness exceeding $10^4\ M^{-1}\ cm^{-1}$.

Its emission wavelength should exceed 550 nm to reduce overlap with sub-cellular (cytoplasmic and mitochondrial) autofluorescence and allow dual-color imaging with EGFP.

The indicator should have enough polar groups, such as carboxylates, to render it highly water soluble but impermeant through lipid membranes, to prohibit dye leakage and compartmentalization.

To permit the simultaneous loading of large cell populations, these polar groups should be maskable by non-polar protection groups, e.g., acetoxymethyl (AM-) esters [31,32], which are hydrolysed inside the cell by esterase activity.

The indicator should ideally display a 'handle' to which site-specific tags can be linked so as to target the molecule to specific sub-cellular compartments.

No such compound has yet been demonstrated to work in living cells, despite ongoing efforts in organic chemical synthesis of long-wavelength emitting dyes [33], genetically targeted Ca^{2+} indicators [34] and biarsenical probes [35].

We now report the synthesis and properties of a non-ratiometric red-emitting indicator meeting these criteria. Compared to the originally described preparation [2], we have streamlined its synthesis by using a commercially available intermediate and thus removing three reaction steps with low yield, resulting in a highly purified preparation of Calcium Ruby that shows a >50-fold peak fluorescence enhancement upon Ca^{2+} binding, while having a similar affinity (29 μM) for Ca^{2+}-binding as the earlier reported preparation [2].

Due to this low affinity, Calcium Ruby monochloride is valuable for measuring large and fast Ca^{2+} transients, but will be largely insensitive below $[Ca^{2+}] \sim 1$ μM. As anticipated, our Calcium Ruby shares many of the advantageous features of its Texas Red™/X-rhod parent fluorophore, with the important additional benefit to be easily attached to any target molecule via its NH_2 end. However, as expected for an extended rhodamine derivative the dye also presents some disadvantages: (i) Although an AM-ester can be synthesized with the carboxylic radicals protected, the resulting ester still bears a positive charge and, like its X-rhod counterparts, is probably less membrane-permeant than its electroneutral fluorescein counterparts. Other problems are (ii) its tendency to stick to the plasma membrane when present in the extracellular saline, (iii) its much reduced dynamic range *in situ* when compared to the good *in vitro* performance, (iv) the difficulty to interpret Calcium Ruby fluorescence in terms of absolute $[Ca^{2+}]$ levels, which is a common problem with non-ratiometric indicators but is accentuated by the mitochondrial sequestration of Calcium Ruby. Like many dyes with a positive charge, (*v*), Calcium Ruby is sequestered into mitochondria, most likely through a combination of its diffusion through membranes, assisted by mitochondrial-membrane potential-driven uptake and hydrophobic interactions [22,33]. In the absence of stimulation, $[Ca^{2+}]_m \approx [Ca^{2+}]_i$, but mitochondria have a high Ca^{2+} capacity and thus can take large Ca^{2+} loads when mopping up excess cytoplasmic Ca^{2+}. Therefore, imaging $[Ca^{2+}]_m$ requires a low-affinity dye. In our hands, Calcium-Ruby is an ideal dye for such measurements.

We designed the Calcium Ruby molecule with a molecular handle to be attached to other biomolecules. This NH_2 linker made it possible to overcome the liability of sub-cellular sequestration by synthesizing a large-MW dextran conjugate. Our demonstration of imaging cytoplasmic Ca^{2+} signals triggering chromaffin-granule secretion with the dextran-linked Calcium Ruby is a first indication of the benefit of this strategy.

We currently synthesize halo- or methyl-substitutions on the BAPTA Ca^{2+} chelating group to generate Calcium Ruby indicators with a wide range of affinities, from ~0.5 to 300 μM [2]. Different conjugations on the binding arm will permit their sub-cellular targeting to restrict the read-out of Ca^{2+} to specific and defined sub-cellular compartments, and thus to tailor EGFP-compatible Ca^{2+} probes to the specific biological application. We expect our Calcium Ruby family to be a versatile toolbox for building red-emitting Ca^{2+} indicators.

Conflict of interest statement

The authors declare no conflicting interest.

Acknowledgements

Supported by the Action Concertée Incitative (ACI) Nanosciences et Nanotechnologies of the French Ministry of Science and Technology and the Groupement d'Intérêt Publique – Agence National de la Recherche (GIP-ANR) PNANO, the European Union (Grant nos. FP6-2004-013880, FP6-2005-019481, FP6-2006-037897, to M.O.), as well as the Bettencourt-Schueller Foundation. CL, AY, SG and DL received postdoctoral fellowships from the Fondation pour la Recherche Médicale (FRM), the Centre National de la Recherche Scientifique (CNRS) and the GIP-ANR, respectively. U.B. and M.P. acknowledge grants from the Deutsche Forschungsgemeinschaft (SFB 530, to U.B.) and HOMFOR. We thank Drs. Isabel Llano, David Ogden, and Nicole Ropert for comments on earlier versions of the manuscript and Dr. Stéphane Supplisson for the loan of equipment.

Appendix A. Supplementary data

Supplementary data associated with this article can be found, in the online version, at doi:10.1016/j.ceca.2008.11.007.

References

[1] S. Bolsover, O. Ibrahim, N. O'luanaigh, H. Williams, S. Cockcroft, Use of fluorescent Ca^{2+} dyes with green fluorescent protein and its variants: problems and solutions, Biochem. J. 356 (2001) 345–352.

[2] S. Gaillard, A. Yakovlev, C. Luccardini, M. Oheim, A. Feltz, J.-M. Mallet, Synthesis and characterization of a new red-emitting Ca^{2+} indicator, Calcium Ruby, Org. Lett. 9 (2007) 2629–2632.
[3] J.A. Titus, R. Haugland, S.O. Sharrow, D.M. Segal, Texas Red, a hydrophilic, red-emitting fluorophore for use with fluorescein in dual parameter flow microfluorometric and fluorescence microscopic studies, J. Immunol. Methods 50 (1982) 193–204.
[4] E. Neher, Concentration profiles of intracellular calcium in the presence of a diffusible chelator, in: Experimental Brain Research, Series 14, Springer Verlag, Berlin, Heidelberg, 1986, pp. 80–96.
[5] E. Neher, Details of Ca^{2+} dynamics matter, J. Physiol. 586. 8 (2008) 2031.
[6] M. Oheim, D. Li, Quantitative colocalisation imaging: concepts, measurements, and pitfalls, in: S.L. Shorte, F. Frischknecht (Eds.), Imaging Cellular and Molecular Biological Function, Springer, New York, Heidelberg, Berlin, 2007.
[7] X. Zhang, J. Rodrigues, L. Evans, B. Hinkle, L. Ballantyne, M. Pena, Formation of urea dipeptides from carbonyldiimidazole: application toward the protease inhibitors GE 20372 and MAPI, J. Org. Chem. 62 (1997) 6420–6423.
[8] F. Bigi, R. Maggi, G. Sartori, Selected syntheses of ureas through phosgene substitutes, Green Chem. 2 (2000) 140–148.
[9] S.P. Rannard, N.J. Davis, I. Herbert, Synthesis of water soluble hyperbranched polyurethanes using selective activation of AB2 monomers, Macromolecules 37 (2004) 9418–9430.
[10] T.E. Proseus, J.S. Boyer, Turgor pressure moves polysaccharides into growing cell walls of *Chara corallina*, Ann. Bot. 95 (2005) 967–979.
[11] R.Y. Tsien, The green fluorescent protein, Annu. Rev. Biochem. 67 (1998) 509–544.
[12] E.M. Nolan, J.W. Ryu, J. Jaworski, R.P. Feazell, M. Sheng, S.J. Lippard, Zinspy sensors with enhanced dynamic range for imaging neuronal cell zinc uptake and mobilization, J. Am. Chem. Soc. 128 (2006) 15517–15527.
[13] R.Y. Tsien, New calcium indicators and buffers with high selectivity against magnesium and protons: design, synthesis, and properties of prototype structures, Biochemistry 19 (1980) 2396–2404.
[14] E.M. Adler, G.J. Augustine, S.N. Duffy, M.P. Charlton, Alien intracellular calcium chelators attenuate neurotransmitter release at the squid giant synapse, J. Neurosci. 11 (1991) 1496–1507.
[15] R.K. Emanus, R. Grunwald, J.J. Lemasters, Rhodamine 123 as a probe of transmembrane potential in isolated rat-liver mitochondria: spectral and metabolic properties, Biochim. Biophys. Acta 850 (1986) 436–448.
[16] J. Sakanoue, K. Ichikawa, Y. Nomura, M. Tamura, Rhodamine 800 as a probe of energization of cells and tissues in the near-infrared region: a study with isolated mitochondria and hepatocytes, Biochem. J. 232 (1997) 29–37.
[17] R.C. Scaduto, L.W. Grotyohann, Measurement of mitochondrial membrane potential using fluorescent rhodamine derivates, Biophys. J. 76 (1999) 469–477.
[18] A.J. Kowaltowski, R.F. Castilho, A.E. Vercesi, Mitochondrial permeability transition and oxidative stress, FEBS Lett. 495 (2001) 12–15.
[19] E. Cadenas, A. Boveris, Enhancement of hydrogen peroxide formation by protophores and ionophores in antimycin-supplemented mitochondria, Biochem. J. 188 (1980) 31–37.
[20] A.U. Abramov, M.R. Duchen, Actions of ionomycin, 4-BrA23187 and a novel electrogenic Ca^{2+} ionophore on mitochondria in intact cells, Cell Calcium 32 (2003) 101–112.
[21] F. Capel, L. Demaison, F. Maskouri, A. Diot, C. Buffière, P. Patureau Mirand, L. Mosoni, Calcium overload increases oxidative stress in old rat gastrocnemius muscle, J. Physiol. Pharmacol. 56 (2005) 369–380.
[22] L.V. Johnson, M.L. Walsh, B.J. Bockus, L.B. Chen, Monitoring of relative mitochondrial membrane potential in living cells by fluorescence microscopy, J. Cell Biol. 88 (1981) 526–535.
[23] J.R. Bunting, T.V. Phan, E. Kamali, R.M. Dowben, Fluorescent cationic probes of mitochondria. Metrics and mechanism of interaction, Biophys. J. 56 (1989) 979–993.
[24] T. Voets, E. Neher, T. Moser, Mechanisms underlying phasic and sustained secretion in chromaffin cells from mouse adrenal slices, Neuron 23 (1999) 607–615.
[25] G.J. Augustine, E. Neher, Calcium requirements for secretion in bovine chromaffin cells, J. Physiol. 450 (1992) 247–271.
[26] H. Plattner, A.R. Artalejo, E. Neher, Ultrastructural organization of bovine chromaffin cell cortex – analysis by cryofixation and morphometry of aspects pertinent to exocytosis, J. Cell Biol. 139 (1997) 1709–1717.
[27] J.A. Steyer, H. Horstmann, W. Almers, Transport, docking and exocytosis of single secretory granules in live chromaffin cells, Nature 388 (1997) 474–478.
[28] M. Oheim, D. Loerke, W. Stühmer, R.H. Chow, The last few milliseconds in the life of a secretory granule. Docking, dynamics and fusion visualized by total internal reflection fluorescence microscopy (TIRFM), Eur. Biophys. J. 27 (1998) 83–98.
[29] U. Becherer, T. Moser, W. Stühmer, M. Oheim, Calcium regulates exocytosis at the level of single vesicles, Nat. Neurosci. 6 (2003) 846–853.
[30] U. Becherer, M. Pasche, S. Nofal, D. Hof, U. Matti, J. Rettig, Quantifying exocytosis by combination of membrane capacitance measurements and total internal reflection fluorescence microscopy in chromaffin cells, PLoS ONE 6 (2007) e505.
[31] R.Y. Tsien, A non-disruptive technique for loading calcium buffers and indicators into cells, Nature 290 (1981) 527–528.
[32] R.Y. Tsien, T. Pozzan, Measurement of cytosolic free Ca^{2+} with quin2, Meth. Enzymol. 172 (1989) 230–262.
[33] M. Poenie, Fluorescent calcium indicators based on BAPTA, in: J.W.J. Putney (Ed.), Calcium Signalling, CRC Press, Boca Raton, 2000, pp. 1–46.
[34] M.G.O. Mank, Genetically encoded calcium indicators, Chem. Rev. 108 (2008) 1550–1564.
[35] O. Tour, S.R. Adams, R.A. Kerr, R.M. Meijer, T.J. Sejnowski, R.W. Tsien, R.Y. Tsien, Calcium Green FlAsH as a genetically targeted small-molecule calcium indicator, Nat. Chem. Biol. 3 (2007) 423–431.